Asymptotic behavior of apparent generalized oscillator strengths for optically forbidden transitions in rare-gas atoms

T. Y. Suzuki, H. Suzuki, and S. Ohtani
Institute for Laser Science, University of Electro-Communications, 1-5-1 Chofugaoka, Chofu, Tokyo 182-8585, Japan

T. Takayanagi and K. Okada
Department of Physic, Sophia University, 7-1 Kioicho, Chiyoda-ku, Tokyo 102-8554, Japan

(Received 3 October 2005; revised manuscript received 31 August 2006; published 7 March 2007)

Apparent generalized oscillator strengths (apparent GOS's) have been measured for three types of optically forbidden transitions in rare-gas atoms as functions of the squared momentum transfer K^2 at small K^2 range ($\leqslant$0.4 a.u.). The apparent GOS's were deduced from the differential cross sections for excitation, which were measured by means of the electron energy-loss spectroscopy. Electron impact energies were 100, 300, and 500 eV, and the scattering angles were from 0.8° to 10°. In the case where the first Born approximation does not hold, the apparent GOS as a function of K^2 (the apparent GOS function) shows characteristic dependence on the electron collision energy according to the character of the transition. In the present observation, for the $np^6\ {}^1S_0 \rightarrow np^5(n+1)p'[1/2]_0$ transitions, the specific behavior has been observed in the apparent GOS functions characteristic of that for the ${}^1S_0 \rightarrow {}^1S_0$ type transition, in which the term symbols of the initial and the final states do not change. For the $np^6\ {}^1S_0 \rightarrow np^5(n+1)p[5/2]_{2,3}$; $[3/2]_{1,2}$ transitions, a certain new type of deviations from the first Born approximation, which is interpreted to be characteristic of the ${}^1S_0 \rightarrow {}^1D_2$ type transition, have been observed in the apparent GOS functions with some modifications depending on respective atomic species. For the $5p^6\ {}^1S_0 \rightarrow 5p^5 5d\ [7/2]_3$; $[5/2]_3$ transitions in Xe, it is observed that the apparent GOS curves have no impact energy dependence for impact energies from 100 eV to 500 eV, which suggests that the first Born approximation is valid for such low impact energies and the curves agree with the Bethe-GOS. It is found that the GOS's varies in proportional to K^4 at small K^2 region ($\leqslant$0.1 a.u.), which suggests that the octupole moment is dominant in these transitions. We interpret that these features of the behavior are specific for the ${}^1S_0 \rightarrow {}^1F_3$ type transition. On the whole, it is found that the behavior of the apparent GOS function can be well understood by considering the main contribution from a certain *LS*-coupling state when the excited state is represented by the intermediate coupling scheme which is expressed as a linear combination of the *LS*-coupled states.

DOI: 10.1103/PhysRevA.75.032705 PACS number(s): 34.80.Dp

I. INTRODUCTION

The generalized oscillator strength (GOS) is a fundamental quantity for atoms and molecules and relates to various physical constants. The GOS has been first introduced by Bethe [1] in 1930 in order to calculate the stopping power of materials for beta rays. Ever since, it has been studied by many investigators theoretically and experimentally [2]. We have made a series of measurements of the GOS in rare-gas atoms mainly for optically allowed transitions, e.g., in Ne [3], Ar [4], Kr [5], and in Xe [6,7].

When the condition for the first Born approximation (FBA) is satisfied, the GOS is obtained directly from the differential cross section (DCS), which is measured by means of the electron scattering experiment, using the general relationship between the GOS and the DCS. However, when the condition for the FBA is not satisfied, the quantity derived from the DCS using the same relationship between the GOS and the DCS, which is called the apparent GOS, does not fully agree with the Bethe-GOS. The behavior of the variation of the apparent GOS as a function of the squared momentum transfer K^2, which we call the apparent GOS function or the apparent GOS curve (against K^2), is dependent on the collision energy and depends upon the nature of the transition concerned, especially for the optically forbidden transitions. Therefore, an accumulation of the knowledge on the features of the behavior of the apparent GOS functions for various typical transitions might be quite useful to identify the character of the transition when it is unknown.

However, very few systematic studies have been available on the variations in the apparent GOS functions for low and intermediate collision energies. For this motivation, we measured the apparent GOS functions for several typical types of optically forbidden transitions in rare-gas atoms, especially in the region of small momentum transfer K^2 ($<$0.4) at collision energies 100, 300, and 500 eV.

The *jl*-coupling designation, which is considered commonly to be suitable to express the low lying excited states in rare-gas atoms, is used here according to the Tables of Atomic Energy Levels by Moore [8]. The transitions measured are as follows.

(1) ${}^1S_0 \rightarrow {}^1S_0$ type transitions:
$2p^6\ {}^1S_0 \rightarrow 2p^5({}^2P_{1/2})3p'[1/2]_0$ transition in Ne;
$3p^6\ {}^1S_0 \rightarrow 3p^5({}^2P_{1/2})4p'[1/2]_0$ transition in Ar;
$4p^6\ {}^1S_0 \rightarrow 4p^5({}^2P_{3/2})5p[1/2]_0$ transition in Kr.

(2) ${}^1S_0 \rightarrow {}^1D_2$ type transitions:
$np^6\ {}^1S_0 \rightarrow np^5({}^2P_{3/2})(n+1)p[5/2]_{2,3}$,
$np^5({}^2P_{3/2})(n+1)p[3/2]_{1,2}$ transitions in Ar(n=3), Kr(n=4), Xe(n=5).

(3) $^1S_0 \rightarrow {}^1F_3$ type transitions:
$5p^6\ {}^1S_0 \rightarrow 5p^5(^2P_{3/2})5d[7/2]_3$, $5p^5(^2P_{3/2})5d[5/2]_3$ transitions in Xe.

A. $^1S_0 \rightarrow {}^1S_0$ type transitions

It is known that the apparent GOS function shows quite distinctive behavior depending on the impact energy in the transitions where the term symbols of the initial and the final states do not change, as the case of the $^1S_0 \rightarrow {}^1S_0$ transitions. The most suitable example may be the behavior of the apparent GOS in the $1\,^1S_0 \rightarrow 2\,^1S_0$ transition in He [9]. In this case, the apparent GOS curves do not converge on the Bethe-GOS curve, which is given by the first Born approximation (FBA), unless the impact energy becomes sufficiently high (>1 keV). The apparent GOS curves are located at positions lower than the Bethe-GOS in the region of K^2 between about 0.1 and 7.0 a.u., for impact energies from 200 eV to 800 eV. For relatively low impact energies, for instance <100 eV, the apparent GOS's have values larger than those of the Bethe-GOS in the region of K^2 smaller than around 0.15 a.u., and the apparent GOS curve shows a maximum at around 0.1 a.u. of K^2.

The $3p'[1/2]_0$ state in Ne is known to be well represented by the *LS*-term $^1S_0$. The $4p'[1/2]_0$ state in Ar has main contribution by the term $^1S_0$ in spite of some mixing of the $^3P_0$ term in the eigenfunction. As for the $5p[1/2]_0$ state in Kr, the $^1S_0$ term must be considered to be mixed to a significant extent with the $^3P_0$ term. These situations may be understood by referring to Table III(A), a part of a summary of intermediate coupling coefficients, which will be presented later for comprehensive discussion in Sec. III.

We have observed remarkable impact energy dependences of the apparent GOS functions characteristic of the $^1S_0 \rightarrow {}^1S_0$ type transitions regardless of some mixing with the $^3P_0$ term in the final state. One of the aim of our measurements is to examine how the behavior of the apparent GOS function changes as the nature of the excited state deviates gradually from the pure $^1S_0$ state.

B. $^1S_0 \rightarrow {}^1D_2$ type transitions

In the present measurements, main contributions to the scattering intensities for the $np[5/2]_{2,3}$ and the $np[3/2]_{1,2}$ excitations are expected to be from excitations to the $np[5/2]_2$ and the $np[3/2]_2$ states, respectively, according to the selection rule for the forward scattering [10]. The $np[5/2]_2$ state is expressed by the linear combination of the $^3D_2$, $^1D_2$, and $^3P_2$ terms in order of the coefficient size [11]. Similarly, the $np[3/2]_2$ state is expressed by the linear combination of the $^3P_2$, $^1D_2$, and $^3D_2$ terms. These situations may be understood by referring to Table III(B).

As the singlet-triplet excitations have no contributions to Born amplitude, GOS's for the transitions to the $np[5/2]_2$ and $np[3/2]_2$ states are attributed to the $^1D_2$ components, and it is expected that the apparent GOS functions have a feature in the impact energy dependence characteristic of the $^1S_0 \rightarrow {}^1D_2$ type transition. It has been observed that the common feature of the behavior of the apparent GOS curves in these transitions, although some modification and deviation from the feature remained depending on the final state and atomic species. The feature is as follows: The apparent GOS curves are situated at positions higher than the Bethe-GOS curves for low impact energies and approach the Bethe-GOS curve moving to lower positions as the impact energy increases, which is remarkably in contrast to the $^1S_0 \rightarrow {}^1S_0$ type transitions. It was found that this feature was clearly reproduced in the apparent GOS curves for the $1\,^1S_0 \rightarrow 3\,^1D_0$ transition in He obtained by deducing from the theoretical data on the DCS's as functions of scattering angles and impact energies.

The origin of variation in the impact energy dependence of the apparent GOS functions, observed for the three atomic species in excitations to the same series of the excited states expressed by the *jl*-coupling scheme, will be discussed in Sec. III later.

C. $^1S_0 \rightarrow {}^1F_3$ type transitions

The $5d[7/2]_3$ and the $5d[5/2]_3$ states in Xe are expressed by the linear combination of the $^1F_3$, $^3D_3$, and $^3F_3$ terms [11], which may be seen in Table III(C). At relatively high impact energy, it is expected that the apparent GOS functions have characteristic behavior of the $^1S_0 \rightarrow {}^1F_3$ type transition because the singlet-triplet transition makes much less contribution to the apparent GOS than that of the singlet-singlet transition. Moreover, the transitions to these states from the ground state are the excitations in which the total angular momentum quantum number J changes by 3 ($\Delta J=3$). In these transitions, no contribution of quadrupole moment is expected to the scattering amplitude in the GOS, and it is expected that the octupole moment has a significant role in the scattering amplitude at small scattering angles. In the present experiment we extended the range of scattering angle to the smaller angles ($\geqslant 0.8°$) compared with our previous work [7] to examine the K^4 dependence of the GOS curve at small K^2 regions and to estimate the electric octupole transition probabilities for both transitions.

We would like to give some discussion on these three transitions after the description of experimental results in Sec. III, comparing them with available experimental and theoretical results by other authors.

II. EXPERIMENTAL METHOD

A. Experimental apparatus

A conventional electron-spectrometry equipment setup in the Institute for Laser Science, the University of Electro-Communications, was used for the measurements of the electron-energy-loss spectra to determine the differential cross sections for excitation of each states of interest. As details of design and performance of the electron spectrometer have been described in the preceding papers, we describe them very briefly here [4,5,9].

This apparatus has been designed to be suitable for the intermediate and low energy collisions. Experiments with chemically active species as target gases, as F_2 molecule, were enabled by use of the differential pumping structure

[12]. The electron spectrometer consists of an electron gun, an energy selector, a collision region, an energy analyzer, and a channel electron multiplier. A set of electrostatic lenses connects each part. Simulated hemispherical analyzers, first designed by Jost [13], are employed for the selector and analyzer. The mean trajectory radius is 50 mm for the selector and 80 mm for the analyzer.

At the collision center, a target atomic beam was crossed with the electron beam at right angles. The target atomic beam effused from a nozzle of 0.5 mm inner diameter and 10 mm length. The whole system was enclosed in a vacuum chamber where the ultimate pressure was about 5×10^{-8} Torr. The pressure when the electron-energy-loss spectrum (EELS) measurements were performed was maintained at less than 1×10^{-5} Torr.

The conventional constant resolution mode, where the deceleration voltage for the scattered electrons was swept keeping the pass energy through the analyzer constant, was used and the typical energy resolution was about 50 meV full width at half maximum (FWHM). The angular resolution of the apparatus has been estimated from the measurement of the angular distribution of the primary electron beam incident from the selector as a function of the rotation angle around 0° position. The angular resolution was estimated to be 0.4° full width at half maximum.

For each energy-loss spectrum, the range of collection energies covered was much less than the collision energies, and the energy-loss spectra were measured under conditions where the chromatic aberration in the electron lens before the analyzer was minimized. Therefore, the peak intensity ratios are considered perfectly to be proportional to the true ratios of the corresponding DCS's. The results of the intensity ratio for each angle and each impact energy have been determined from an average of the intensity ratios obtained from three or four independent measurements.

B. Experimental procedures

The absolute DCS's for the inelastic scattering $(d\sigma/d\Omega)_{\text{inel}}$ were deduced from the intensity ratio $(I_{\text{inel}}/I_{\text{el}})$ using the absolute DCS's for the elastic scattering $(d\sigma/d\Omega)_{\text{cl}}$ as the normalization standard, following the relation

$$\left(\frac{d\sigma}{d\Omega}\right)_{\text{inel}} = \frac{I_{\text{inel}}}{I_{\text{el}}}\left(\frac{d\sigma}{d\Omega}\right)_{\text{el}}, \tag{1}$$

where I_{inel} and I_{el} are the scattering intensities which were obtained by the corresponding peak area in the energy loss spectra for the inelastic and elastic scattering, respectively. The absolute elastic scattering cross sections which were adopted as normalization standards were obtained from the data published by other authors [14–19]. The reference numbers of papers from which we obtained the standard absolute cross sections are listed in Table I for each rare-gas atom. The actual zero scattering angle has been calibrated using the symmetrical nature of the intensity ratio $I_{\text{inel}}/I_{\text{el}}$ around 0°. The $(d\sigma/d\Omega)_{\text{el}}$ were obtained by a calculation using a semiempirical fitting function which was based on the data of the absolute elastic scattering cross sections. The fitting function is as follows:

TABLE I. Reference numbers of papers from which the absolute elastic collision DCS's were adopted as the normalization standard.

E_i (eV)	Ne	Ar	Kr	Xe
100	[14,15,18,19]	[14,15]	[14,16]	[14,16]
300	[15,17,19]	[15,17]	[16,17]	[16,17]
500	[15,17,19]	[15,17]	[16,17]	[16,17]

$$\ln\left(\frac{d\sigma}{d\Omega}\right)_{\text{el}} = c_0 + c_1 K + c_2 K^2 + c_3 K^3, \tag{2}$$

where c_0, c_1, c_2, and c_3 are the fitting parameters and K is the absolute value of the momentum transfer vector. Using Eq. (1), the $(d\sigma/d\Omega)_{\text{inel}}$ can be determined by multiplying the intensity ratio with the $(d\sigma/d\Omega)_{\text{el}}$.

For measurements at small scattering angles, the angular resolution cannot be neglected. Using a procedure described in the previous paper [9], we estimated the effect of the finite angular resolution and applied appropriate corrections to both the values of the cross section and the scales of the angle.

The apparent generalized oscillator strength F_{0l}^{ap} is obtained from the differential cross section $(d\sigma/d\Omega)_{\text{inel}}$ as follows:

$$F_{0l}^{\text{ap}}(K,E_i) = \frac{W}{2}\frac{k_0}{k_l}K^2\left(\frac{d\sigma}{d\Omega}\right)_{\text{inel}} \quad \text{(in a.u.)}, \tag{3}$$

where W is an excitation energy and k_0 and k_l are the momenta of the incident and scattered electrons, respectively.

The results are fitted with an expansion formula that is applicable even for non-Born cases [20]

$$F_{0l}^{\text{ap}}(K,E_i) = \frac{1}{1+x^2}\sum_{n=0}^{m} a_n\left(\frac{x}{\sqrt{1+x^2}}\right)^n, \tag{4}$$

where a_n are the fitting parameters and the variable x is equal to $K/[\sqrt{2I}+\sqrt{2(I-W)}]$, here I is the ionization potential and W is the excitation energy.

The apparent GOS's for the $3p'[1/2]_0$ excitation in Ne, for the $4p'[1/2]_0$ excitation in Ar, and the $5p[1/2]_0$ excitation in Kr have been measured at 100, 300, and 500 eV

TABLE II. Summary of experimental errors.

Final state(s)	E_i=100 eV	E_i=300 eV	E_i=500 eV
$3p'[1/2]_0$ in Ne	10%	11%	12%
$4p'[1/2]_0$ in Ar	10%	12%	12%
$5p[1/2]_0$ in Kr	10%	11%	13%
$4p[5/2]_{2,3}$, $4p[3/2]_{1,2}$ in Ar	10%	11%	12%
$5p[5/2]_{2,3}$, $5p[3/2]_{1,2}$ in Kr	10%	10%	13%
$6p[5/2]_{2,3}$, $6p[3/2]_{1,2}$ in Xe	10%	10%	13%
$5d[7/2]_3$ in Xe	10%	10%	13%
$5d[5/2]_3$ in Xe	10%	10%	13%

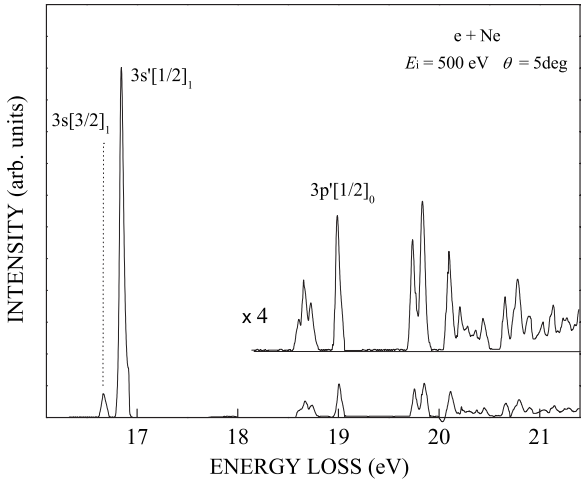

FIG. 1. A typical electron-energy-loss spectrum of Ne for the impact energy 500 eV at the scattering angle 5°.

impact energies. The scattering angles in these measurements were from 0.8° to 12°.

The measurements for the $np[5/2]_{2,3}$ and the $np[3/2]_{1,2}$ excitations ($n=4$ in Ar, $n=5$ in Kr, and $n=6$ in Xe) have been performed for the impact energies of 100, 300, and 500 eV at the scattering angles from 0.8° to 9°. In Ne, two peaks in an electron-energy-loss spectrum corresponding to these excitations were too close to resolve for this apparatus. The DCS's and the apparent GOS's for the $5d[7/2]_3$ and the $5d[5/2]_3$ excitations in Xe have been measured for the impact energies 100, 300, and 500 eV at the scattering angles from 0.8° to 9°. The experimental errors in the results of the apparent GOS's for the $3p'[1/2]_0$ excitation in Ne at 500 eV are estimated to be less than ±12%. This value is deduced as the quadratic sum of the statistical error 8% in the intensity ratios, systematic error 5% caused by the effect of the limited energy resolution, angular resolution, and the angle calibration and others, and the error 7% in the standard absolute values of the elastic DCS.

The experimental errors in the results of the apparent GOS's were estimated based on the similar manner for all other excitation processes and at the other impact energies. These estimated experimental errors are listed in Table II for each excited state at three impact energies.

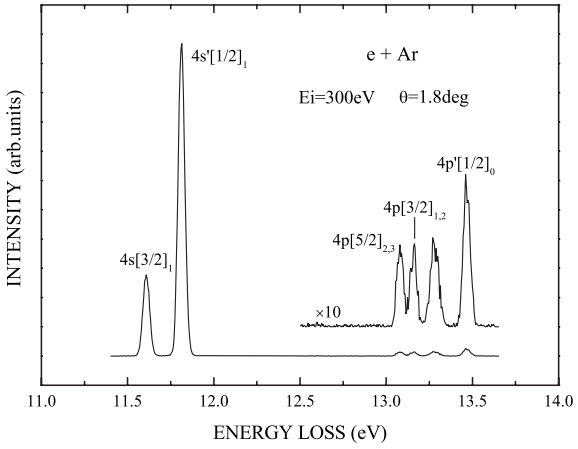

FIG. 2. A typical electron-energy-loss spectrum of Ar for the impact energy 300 eV at the scattering angle 1.8°.

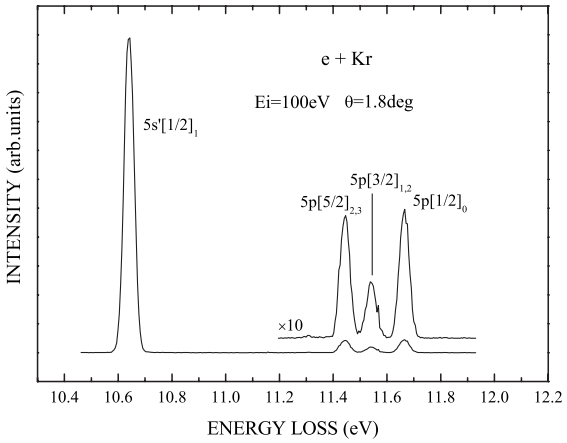

FIG. 3. A typical electron-energy-loss spectrum of Kr for the impact energy 100 eV at the scattering angle 1.8°.

III. RESULTS AND DISCUSSION

Examples of typical EELS are shown in Fig. 1, Fig. 2, Fig. 3, and Fig. 4, for Ne, Ar, Kr, and Xe, respectively. The impact energy and the scattering angle for each spectrum are described in each figure caption. The spectral peaks corresponding to the optically forbidden transitions of the present interests are designated with the term symbols in the *jl*-coupling notation. Several other notable peaks due to optically allowed transitions are also specified with the term symbols in the same scheme.

The intermediate coupling coefficients of the *LS* components for the states of the present interests, which were calculated by several authors, are listed in Table III with references for the following discussion.

A. $^1S_0 \rightarrow {}^1S_0$ type transitions

In Fig. 1, the spectrum of Ne, a peak at 18.966 eV corresponds to the $3p'[1/2]_0$ excitation. In Fig. 2 for the Ar spec-

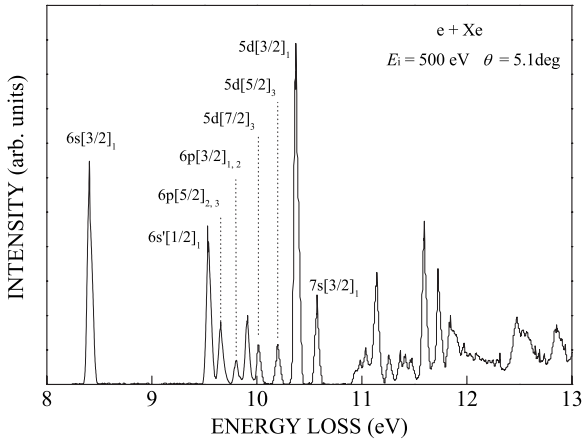

FIG. 4. A typical electron-energy-loss spectrum of Xe for the impact energy 500 eV at the scattering angle 5.1°.

TABLE III. Summary of intermediate coupling coefficients. The last column presents a reference number.

		Reference
	(A) $^1S_0 \rightarrow {}^1S_0$ type transition	
Ne $3p'[1/2]_0$	$0.99(2p^5 3p:{}^1S_0)+0.14(2p^5 3p:{}^3P_0)$	Machado (1984) [33]
	$0.9452(2p^5 3p:{}^1S_0)-0.2690(2p^5 4p:{}^1S_0)$ $-0.1165(2p^5 5p:{}^1S_0)$	Cheng (2005) [22]
Ar $4p'[1/2]_0$	$0.9313(3p^5 4p:{}^1S_0)+0.2862(3p^5 4p:{}^3P_0)$ $-0.1891(3p^5 5p:{}^1S_0)$	Zhu (2006) [24]
Kr $5p[1/2]_0$	$0.7238(4p^5 5p:{}^1S_0)-0.6828(4p^5 5p:{}^3P_0)$	Guo (2005) [34]
	$0.7126(4p^5 5p:{}^1S_0)-0.6859(4p^5 5p:{}^3P_0)$	Cheng (2005) [29]
	(B) $^1S_0 \rightarrow {}^1D_2$ type transition	
Ar $4p[5/2]_2$	$0.7993(3p^5 4p:{}^3D_2)+0.5839(3p^5 4p:{}^1D_2)$ $-0.1409(3p^5 4p:{}^3P_2)$	Zhu (2006) [24]
Kr $5p[5/2]_2$	$0.7068(4p^5 5p:{}^3D_2)+0.6873(4p^5 5p:{}^1D_2)$ $-0.1666(4p^5 5p:{}^3P_2)$	Guo (2000) [34]
	$0.7143(4p^5 5p:{}^3D_2)-0.6801(4p^5 5p:{}^1D_2)$ $+0.1642(4p^5 5p:{}^3P_2)$	Cheng (2005) [29]
Xe $6p[5/2]_2$	$0.70(5p^5 6p:{}^3D_2)+0.68(5p^5 6p:{}^1D_2)-0.21(5p^5 6p:{}^3P_2)$	Khakoo (1996) [11]
	(B) $^1S_0 \rightarrow {}^1D_2$ type transition	
Ar $4p[3/2]_2$	$0.7524(3p^5 4p:{}^3P_2)+0.5878(3p^5 4p:{}^1D_2)$ $-0.2967(3p^5 4p:{}^3D_2)$	Zhu (2006) [24]
Kr $5p[3/2]_2$	$0.8742(4p^5 5p:{}^3P_2)+0.4343(4p^5 5p:{}^1D_2)$ $-0.2163(4p^5 5p:{}^3D_2)$	Guo (2000) [34]
	$0.8661(4p^5 5p:{}^3P_2)+0.4455(4p^5 5p:{}^1D_2)$ $+0.2251(4p^5 5p:{}^3D_2)$	Cheng (2005) [29]
Xe $6p[3/2]_2$	$0.88(5p^5 6p:{}^3P_2)+0.45(5p^5 6p:{}^1D_2)-0.18(5p^5 6p:{}^3D_2)$	Khakoo (1996) [11]
	(C) $^1S_0 \rightarrow {}^1F_3$ type transition	
Xe $5d[7/2]_3$	$0.76(5p^5 5d:{}^3F_3)+0.60(5p^5 5d:{}^1F_3)-0.23(5p^5 5d:{}^3D_3)$	Khakoo (1996) [11]
	(C) $^1S_0 \rightarrow {}^1F_3$ type transition	
Xe $5d[5/2]_3$	$0.83(5p^5 5d:{}^3D_3)+0.53(5p^5 5d:{}^1F_3)-0.17(5p^5 5d:{}^3F_3)$	Khakoo (1996) [11]

trum, a peak at 13.480 eV corresponds to the $4p'[1/2]_0$ excitation, and in Fig. 3 for the Kr spectrum, a peak at 11.666 eV corresponds to the $5p[1/2]_0$ excitation.

The apparent GOS's for the $3p'[1/2]_0$ excitation in Ne are plotted in Fig. 5 as functions of the squared momentum transfer K^2 for the impact energies 100, 300, and 500 eV. Fitting curves calculated using the expansion formula Eq. (4) are also drawn through the data points. The experimental data measured at 100 eV by Register *et al.* [21] and those at 2500 eV by Cheng *et al.* [22] are also shown. The apparent GOS curves for the $4p'[1/2]_0$ excitation in Ar are drawn in Fig. 6. An experimental data point by Chutjian and Cartwright [23] at 100 eV and the GOS curve by Zhu *et al.* at 2500 eV [24] are also shown. The apparent GOS curves for the $5p[1/2]_0$ excitation in Kr are plotted in Fig. 7. Experimental results measured at the impact energy 2500 eV by Li *et al.* [25] are also presented in Fig. 7.

The present apparent GOS's for all three excitations show a similar distinct impact energy dependence. The apparent GOS's increase as the impact energy increases from 300 to 500 eV in the region of K^2 larger than around 0.05 to 0.07 a.u., and have a broad maximum at K^2 around 0.4 for Ne, at around 0.25 for Ar, and at around 0.2 for Kr. The apparent GOS curves appear to approach asymptotically a certain curve, which should be the Bethe-GOS curve, as the impact energies are increased.

In practice, the present apparent GOS curves appear to approach asymptotically the data points and the fitting curves by Cheng *et al.* [22], Zhu *et al.* [24], and Li *et al.* [25] for Ne, Ar and Kr, respectively, which are reasonably expected to be the Bethe-GOS curve, though in the case of Ne, the maximum of the GOS curve is outside the figure and has a value of 0.0215 at $K^2 \sim 0.5$.

For the impact energy 100 eV, the apparent GOS's increase as K^2 decreases from 0.2 to smaller region, and have a broad maximum at around 0.1 of K^2 in Ne. The similar maximum is observed for Ar at around 0.04 of K^2, and for Kr at around 0.03 of K^2 as shown by fitted curves in the figures. The values of these maxima in the apparent GOS for 100 eV

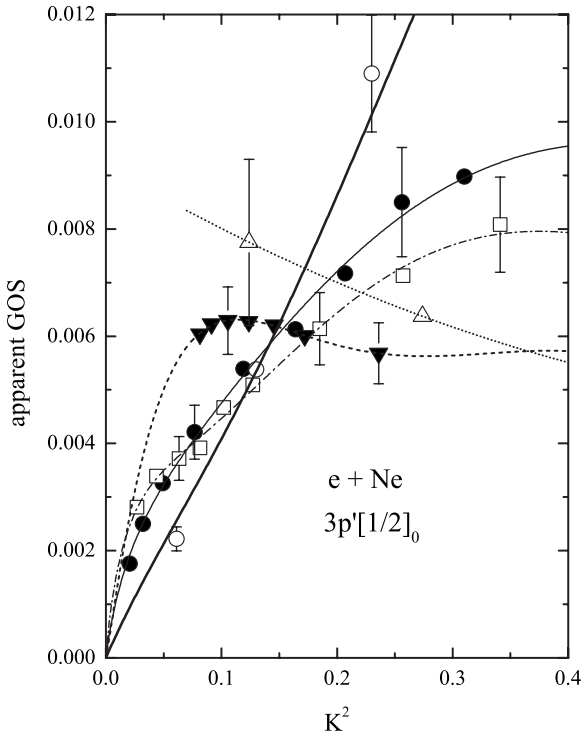

FIG. 5. The apparent GOS for the $3p'[1/2]_0$ excitation in Ne as functions of the squared momentum transfer K^2 for the impact energies of 100 (▼), 300 (□), and 500 eV (●). Experimental data of Register *et al.* (△) at 100 eV [21] and those of Cheng *et al.* (○) at 2500 eV [22] are also plotted.

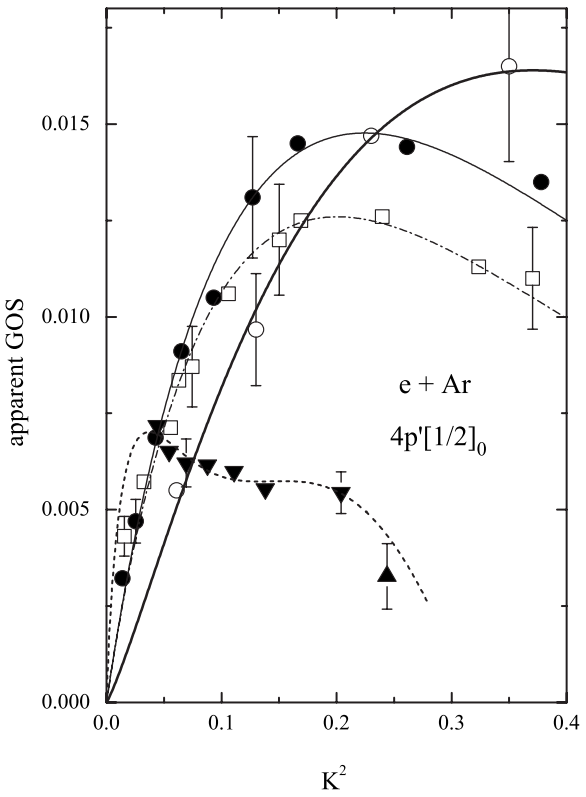

FIG. 6. The apparent GOS for the $4p'[1/2]_0$ excitation in Ar as functions of the squared momentum transfer K^2 for the impact energies of 100 (▼), 300 (□), and 500 eV (●). Experimental data of Chutjian and Cartwright (▲) at 100 eV [23] and by Zhu *et al.* (○) at 2500 eV [24] are also plotted.

are much smaller than the maximum values for higher impact energies. It is notable that overall behavior of the apparent GOS curve appears to be shifted toward smaller K^2 for the case of Ar and Kr, compared with that of Ne. Ionization potential of Ne is 21.56 eV, and fairly larger than those of Ar and Kr, 15.76 and 14.00 eV, respectively. This means that space wave functions of Ar and Kr have broader spread compared with that of Ne. The tendency of the apparent GOS's described above might be considered to reflect the broader spread of the space wave functions in heavier atoms, because the GOS corresponds to Fourier transform of the product of the initial and the final wave functions.

The results by Register *et al.* in Ne are about 20% larger than the present work at 100 eV but within the sum of both experimental errors. The result determined by Chutjian and Cartwright at 100 eV at 10° in Ar is small compared with ours.

It is well known that the higher order Born amplitudes give the main contribution to the apparent GOS for transitions in which the terms of the initial and final states are the same, as the case of the $^1S_0 \rightarrow {}^1S_0$ transition. In this case, larger deviations from the first Born approximation is to be expected unless the impact energies become sufficiently high.

A typical example is $1^1S_0 \rightarrow 2^1S_0$ transition in He. We have made detailed measurements on the apparent GOS's for the $1^1S \rightarrow 2^1S$ and 3^1S transitions previously [9]. It was found that the apparent GOS's for both transitions show the same behavior. The apparent GOS curves approach asymptotically the Bethe-GOS curve, which has a broad maximum at around 1 a.u. of K^2, as the impact energy increases. However, the impact energy should be very high in order to reach the Bethe-GOS curve for the apparent GOS's. In fact, deviation from the FBA has been observed for $1^1S \rightarrow 2^1S$ transition in He even at 800 eV [9]. For the impact energy 100 eV, the apparent GOS's increase gradually as the K^2 decreases from around 2 to 0.1 of K^2, and has a maximum around at 0.1 of K^2. Moreover, it was reported that the similar features were observed for molecules in the case of $X\ ^1\Sigma_g^+ \rightarrow a''\ ^1\Sigma_g^+$ in N_2 [26] and $X\ ^1\Sigma^+ \rightarrow B\ ^1\Sigma^+$ in CO [27].

In Table III, it is found that the $3p'[1/2]_0$ state in Ne is well represented by the *LS* term $^1S_0$. However, the $4p'[1/2]_0$ state in Ar and the $5p[1/2]_0$ state in Kr cannot be represented only by the term $^1S_0$ but some extent of mixing of the $^3P_0$ state must be considered. In spite of this situation, the behavior of the apparent GOS functions for these three states can be commonly interpreted well as the same $^1S_0 \rightarrow {}^1S_0$ type transition, i.e., the $^1S_0$ component in the excited state plays the leading part and the contribution from the $^3P_0$ component might be negligibly small.

B. $^1S_0 \rightarrow {}^1D_2$ type transitions

In Fig. 2, a peak at about 13.095 eV corresponds to the $4p[5/2]_{2,3}$ states, and a peak at about 13.171 eV corresponds to the $4p[3/2]_{1,2}$ states in Ar. In Fig. 3, a peak at about

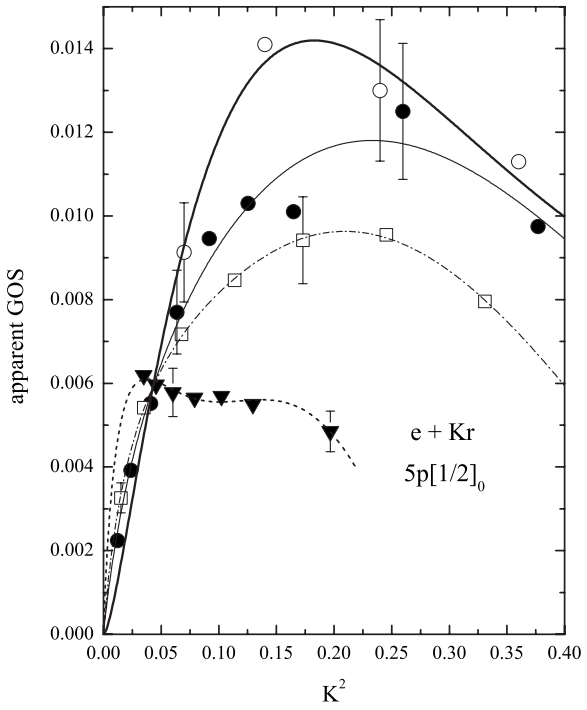

FIG. 7. The apparent GOS for the $5p[1/2]_0$ excitation in Kr as functions of the squared momentum transfer K^2 for the impact energies of 100 (▼), 300 (□), and 500 eV (●). Experimental data of Li *et al.* (○) [25] are also plotted.

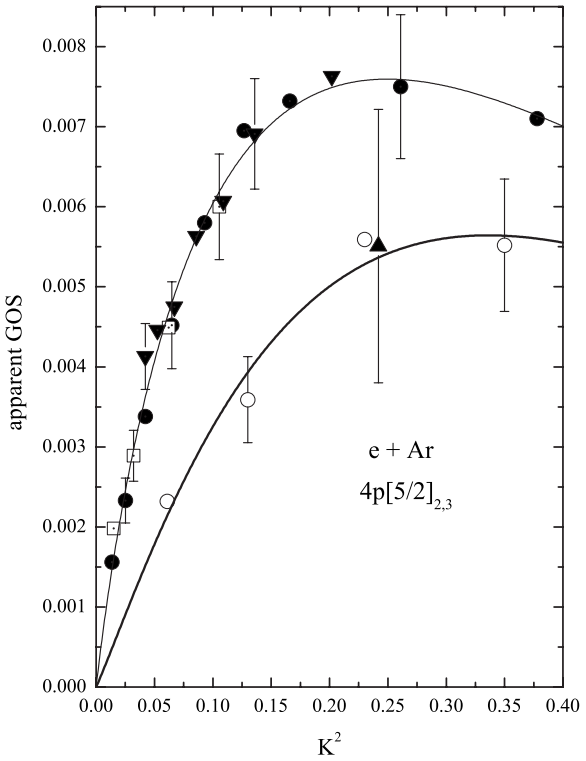

FIG. 8. The apparent GOS for the $4p[5/2]_{2,3}$ excitation in Ar as functions of the squared momentum transfer K^2 for the impact energies of 100 (▼), 300 (□), and 500 eV (●). Experimental results by Chutjian and Cartwright (▲) at 100 eV [23] and by Zhu *et al.* (○) at 2500 eV [24] are also presented.

11.444 eV corresponds to the $5p[5/2]_{2,3}$ states, and a peak at about 11.546 eV corresponds to the $5p[3/2]_{1,2}$ states in Kr. In Fig. 4, a peak at about 9.685 eV corresponds to the $6p[5/2]_{2,3}$ states, and a peak at about 9.821 eV corresponds to the $6p[3/2]_{1,2}$ states in Xe. In these EELS, the energy differences between the states of different J quantum numbers could not be resolved.

The apparent GOS's for the $4p[5/2]_{2,3}$ and $4p[3/2]_{1,2}$ excitations in Ar are plotted in Fig. 8 and Fig. 9, respectively, as functions of the momentum transfer K^2 for impact energies 100, 300, and 500 eV. An experimental datum by Chutjian and Cartwright at 100 eV [23] and the GOS data measured at 2500 eV by Zhu *et al.* [24] are also presented. The results of Chutjian and Cartwright for both excitations are smaller than those at 100 eV in the present work. Impact energy dependences of the apparent GOS's for these states are so small in the energy region 100–500 eV that all data points seem to lie on a single curve within experimental errors. The curves could be expected to be the Bethe-GOS ones, however, it is not necessarily the case because the values measured by Zhu *et al.* 2500 eV are smaller than ours. If the results by Zhu *et al.* present the Bethe-GOS curves, it must be interpreted that the apparent GOS functions for both excitations converge very slowly on the Bethe-GOS from the larger value side, as the impact energy increases.

The present apparent GOS's for the $5p[5/2]_{2,3}$ and the $5p[3/2]_{1,2}$ excitations in Kr measured at the impact energies of 100, 300, and 500 eV are plotted in Fig. 10 and Fig. 11, respectively. The experimental results of Li *et al.* [25], which were measured using 2500 eV impact energy, are also drawn in both figures. In both figures the clear features are observed: The apparent GOS curves for low impact energies have larger values than those for higher impact energies. In other words, the apparent GOS curves are situated at higher positions for low impact energies, as especially indicated in the case of the $5p[3/2]_{1,2}$, although some scatter of data points obscure the clarity in the case of $5p[5/2]_{2,3}$. It may be reasonable to interpret that the apparent GOS's have greater values for low impact energies, and they become smaller and approach the Bethe-GOS values as the impact energy increases. In both transitions, the curves measured by Li *et al.* are considered to be the Bethe-GOS curve. The difference between the curves of the apparent GOS's obtained for the impact energies 100, 300, 500, and 2500 eV (Li *et al.*) is evidently perceived, especially for the $5p[3/2]_{1,2}$. This shows that the first Born approximation is not yet valid for the $5p[5/2]_{2,3}$ and $5p[3/2]_{1,2}$ excitations in the impact energy range from 100 to 500 eV.

The apparent GOS's for the $6p[5/2]_{2,3}$ and the $6p[3/2]_{1,2}$ excitations in Xe are presented in Fig. 12 and Fig. 13, respectively, for impact energies of 100, 300, and 500 eV. For both excitations, behavior of the impact energy dependence of the apparent GOS curves is very similar with those for the excitations in the same series of Kr, and the difference between the apparent GOS's at 100, 300, and 500 eV is clear. It is suggested that the first Born approximation does not hold also for the same sort of excitations in Xe at these impact energies, although for the present no experimental data are available on the Bethe-GOS curves in the case of Xe.

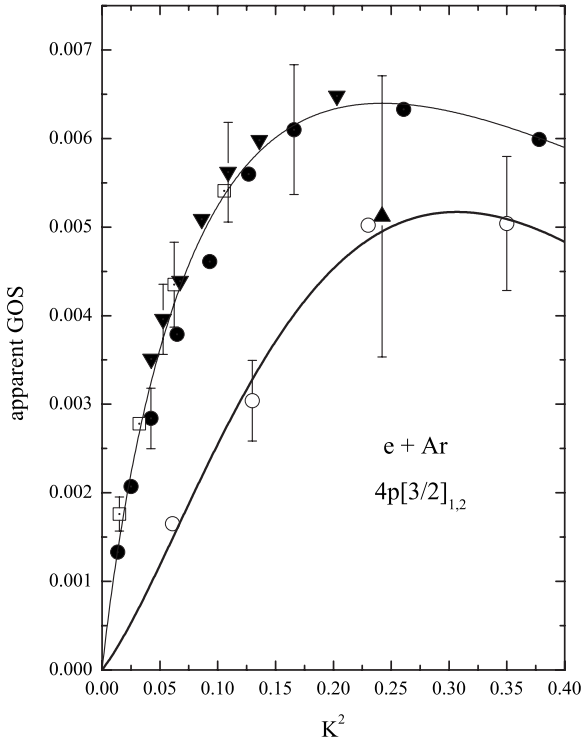

FIG. 9. The apparent GOS for the $4p[3/2]_{1,2}$ excitation in Ar as functions of the squared momentum transfer K^2 for the impact energies of 100 (▼), 300 (□), and 500 eV (●). Experimental results by Chutjian and Cartwright (▲) at 100 eV [23] and by Zhu *et al.* (○) at 2500 eV [24] are also presented.

As observed above, it is found that the degree of the deviation from the first Born approximation is different in excitations of the states which belong to the same series expressed by the *jl*-coupling scheme. As an overall tendency, the apparent GOS's for both transitions at the energies between 100 eV and 500 eV are significantly larger than the Bethe-GOS curves and gradually decrease to converge on the Bethe-GOS's as the impact energy increases.

It can be considered that main contribution to each apparent GOS is caused by the excitation to the $np[5/2]_2$ and the $np[3/2]_2$ states, respectively, according to the selection rule for forward electron scattering as follows: Zero angle (and 180°) scattering is forbidden if $L_i+p_i+L_f+p_f$ is odd. Here L_i and L_f are the angular momenta and p_i and p_f are the parity numbers of the initial and final electronic states of the atom, respectively [10].

The $np[5/2]_2$ states are represented in the intermediate coupling by the linear combination of the $^3D_2$, $^1D_2$, and $^3P_2$ terms in the *LS*-coupled scheme. The coefficients for the $^3D_2$ term are slightly greater than those for the $^1D_2$ term, and those for the $^3P_2$ term are rather smaller than those for the other two terms, for the three atomic species (cf. Table III). The $np[3/2]_2$ states are also represented by the linear combination of the $^3P_2$, $^1D_2$, and $^3D_2$ terms. However, the coupling coefficients for the $^3P_2$ term are considerably larger than those for the $^1D_2$ and $^3D_2$ terms, those for the $^1D_2$ term being about twice larger than those for the $^3D_2$ term (cf. Table III).

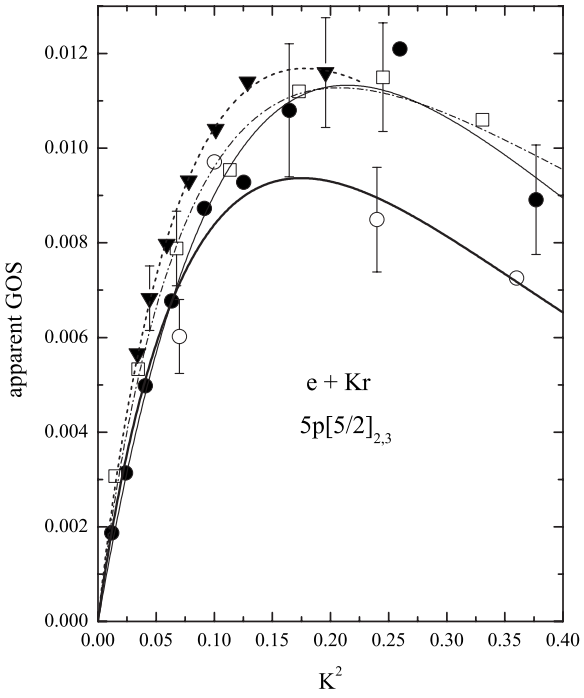

FIG. 10. The apparent GOS for the $5p[5/2]_{2,3}$ excitation in Kr as functions of the squared momentum transfer K^2 for the impact energies of 100 (▼), 300 (□), and 500 eV (●). Experimental results by Li *et al.* (○) at 2500 eV [25] are also presented.

In the $np[5/2]_2$ and the $np[3/2]_2$ states in Ar, Kr, and Xe, the only component of the *LS*-coupled term with the singlet multiplicity is the $^1D_2$ term. Considering the singlet nature of

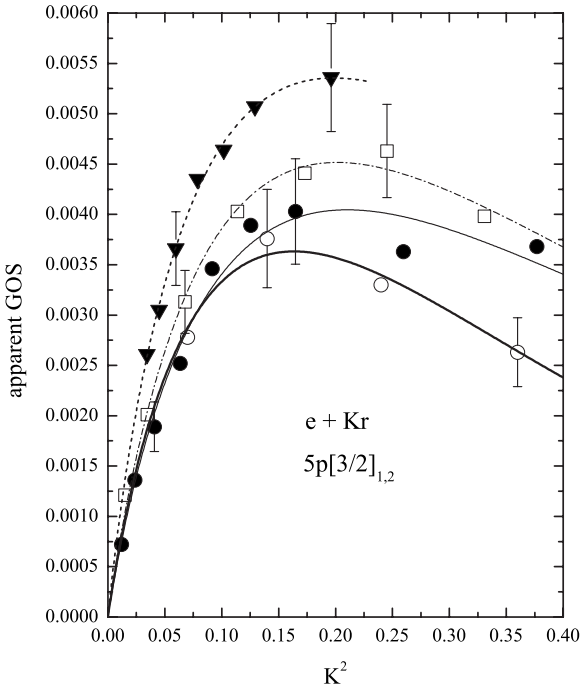

FIG. 11. The apparent GOS for the $5p[3/2]_{1,2}$ excitation in Kr as functions of the squared momentum transfer K^2 for the impact energies of 100 (▼), 300 (□), and 500 eV (●). Experimental results by Li *et al.* (○) at 2500 eV [25] are also presented.

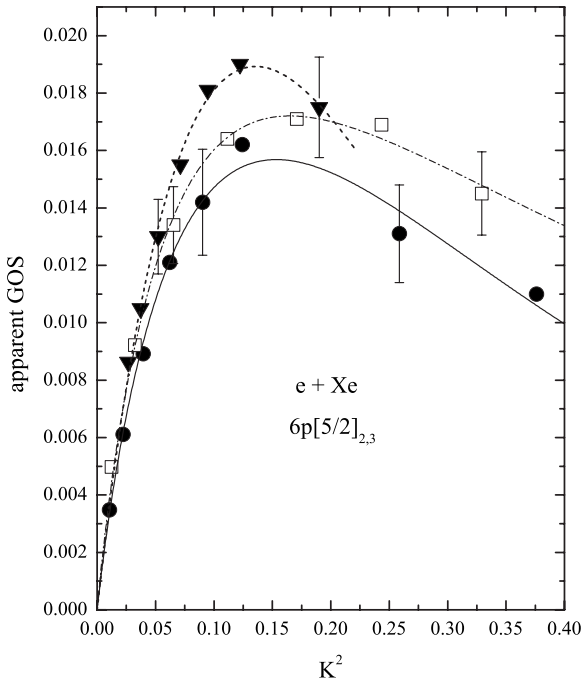

FIG. 12. The apparent GOS for the $6p[5/2]_{2,3}$ excitation in Xe as functions of the squared momentum transfer K^2 for the impact energies of 100 (▼), 300 (□), and 500 eV (●).

the ground state, the $^1S_0$ in the rare-gas atoms, it is expected that the dominant contribution in the transition must be the component of the *LS* term $^1D_2$. At present, no experimental data are available on the behavior of the apparent GOS function for the $^1S_0 \rightarrow {}^1D_2$ type transition in rare-gas atoms. A

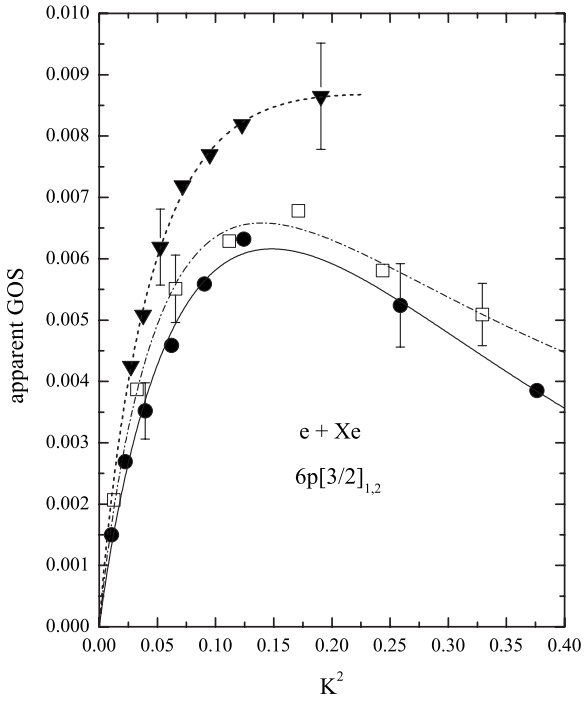

FIG. 13. The apparent GOS for the $6p[3/2]_{1,2}$ excitation in Xe as functions of the squared momentum transfer K^2 for the impact energies of 100 (▼), 300 (□), and 500 eV (●).

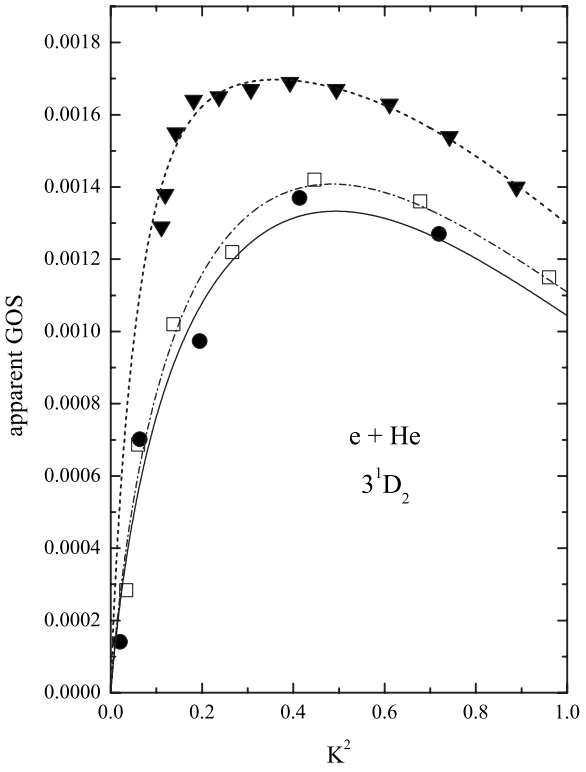

FIG. 14. The apparent GOS for the $1^1S_0 \rightarrow 3^1D_2$ excitation in He as functions of the squared momentum transfer K^2 for the impact energies of 100 (▼), 300 (□), and 500 eV (●). The data are converted from theoretical results of the DCS's calculated using a generalized distorted wave method based on the second order potential equations by Winters *et al.* [28].

typical behavior of apparent GOS curves for the $^1S_0 \rightarrow {}^1D_2$ transition could be found at the $1^1S_0 \rightarrow 3^1D_2$ transition in He. However, experimental results on the DCS of the excitation of the $1^1S_0 \rightarrow 3^1D_2$ transition in He have never been obtained by any experimental studies, because in the EELS measurements the energy-loss peak corresponding the 3^1D_2 excitation (23.073 eV) could not be resolved from the peak for the 3^1P_1 (23.086 eV), which has much higher intensity than that for the 3^1D_2 excitation. We have tried to deduce the apparent GOS's from theoretical DCS's for the impact energies 100–500 eV. The results converted from the data calculated by means of the generalized distorted wave method based on the second order potential equations by Winters, Issa, and Bransden [28] are presented in Fig. 14. This figure shows that, in the $1^1S_0 \rightarrow 3^1D_2$ excitation in He, the apparent GOS curves are situated at higher positions for the low impact energies, and move to lower positions as the impact energy increases, approaching the Bethe-GOS curve. This sort of overall tendency of the impact energy dependence of the apparent GOS function is common through the transitions of the present interests.

It suggests that the main character of the $np[5/2]_2$ and $np[3/2]_2$ excitations in Ar, Kr, and Xe should be interpreted to be the $^1S_0 \rightarrow {}^1D_2$ type transition. However, some discrepancies in shapes of the apparent GOS curves are observed between those for different atomic species, especially for the $np[5/2]_{2,3}$ excitations in Kr and Xe. The cause of the dis-

crepancies may be partly attributable to the contribution from the electron exchange components such as the $^1S_0 \rightarrow {}^3P_2$ or $^3D_2$ transitions. Other some contribution may be possible from the components involved in other states, unresolved from the $J=2$ peak of the present interests in the EELS, such as the $np[5/2]_3$ and $np[3/2]_1$ states.

C. $^1S_0 \rightarrow {}^1F_3$ type transitions

In Fig. 4, peaks at 10.039 eV and 10.220 eV correspond to excitations to the $5d[7/2]_3$ and the $5d[5/2]_3$ states in Xe, respectively.

In our previous paper, we have already presented the apparent GOS curves for the excitations $5p^6 {}^1S_0 \rightarrow 5p^5 5d[7/2]_3$, $5p^5 5d[5/2]_3$ in Xe, which were deduced from the measurements of DCS's for impact energies 400 and 500 eV at scattering angles from 2.4° to 15°. For both excitations, all data points for the different impact energies lay on a single curve, which suggested well that the measured apparent GOS curves agreed with the respective Bethe-GOS curves. Both GOS curves showed characteristic broad profiles with the maxima at around $K^2 \approx 0.8$ [7].

Cheng *et al.* obtained the results for the GOS curves for the $5p'[3/2]_2$ and $4d[7/2]_3$ excitations and for the $5p'[1/2]_0$ and $4d[5/2]_3$ excitations in Kr separately by the fast electron collisions (2500 eV), although these two states each could not be resolved in their energy-loss peaks [29]. In order to separate the GOS's for the two states, they used a discrimination procedure that was based on the selectivity for excitation to the singlet component reflecting the singlet nature of the ground state and on the idea that the GOS is proportional to the square of the intermediate coefficient of the singlet component. They observed that the GOS curves for the $4d[7/2]_3$ and the $4d[5/2]_3$ excitations showed broad profiles with their maxima at around $K^2 \approx 0.8$. They pointed out that the behavior was very similar to that for the $5d[7/2]_3$ and $5d[5/2]_3$ excitations in Xe, which were observed by Suzuki *et al.* [7]. They concluded that this behavior might be a typical one characteristic of the electric octupole transitions.

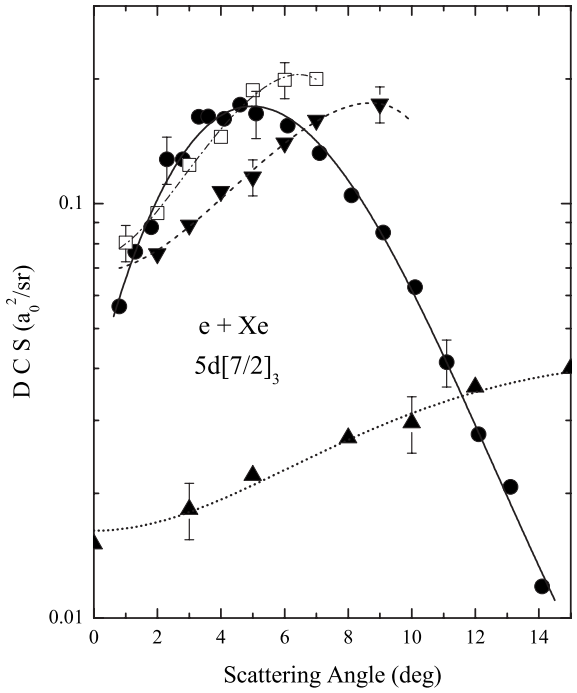

FIG. 15. The DCS's for the $5d[7/2]_3$ excitation in Xe as a function of the scattering angle for the impact energies of 100 (▼), 300 (□), and 500 eV (●). Experimental results of Khakoo *et al.* (▲) [30] for the impact energy of 30 eV are also plotted.

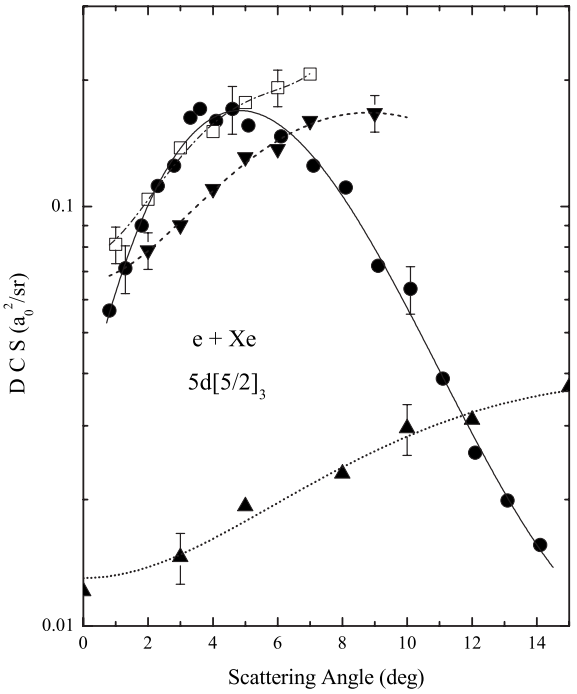

FIG. 16. The DCS's for the $5d[5/2]_3$ excitation in Xe as a function of the scattering angle for the impact energies of 100 (▼), 300 (□), and 500 eV (●). Experimental results of Khakoo *et al.* (▲) [30] at 30 eV are also plotted.

In the present work, we extended the measurements of the DCS's for the excitations $5p^6 {}^1S_0 \rightarrow 5p^5 5d[7/2]_3$, $5p^5 5d[5/2]_3$ in Xe from 3.3° to 0.8°, in order to examine the behavior in the region of $K^2 \rightarrow 0$ in more detail. We show the DCS's for the excitation to these states in Fig. 15 and Fig. 16, respectively, for the impact energies of 100, 300, and 500 eV as functions of the scattering angle. The data points for 500 eV at angles less than 3.3° are present results and those at larger angles are the previous ones. Experimental results by Khakoo *et al.* [30] at 30 eV are also plotted in both figures.

Most prominent feature in the DCS's for the $5d[7/2]_3$ and $5d[5/2]_3$ excitations is rapid decrease of the DCS at forward scattering angles. This feature is observed for the impact energies from 30 eV to 500 eV. Moreover it is assumed that the maximum in the DCS's shifts toward larger scattering angles as the impact energy decreases.

The apparent GOS's in the range of small K^2 (<0.4) for the $5d[7/2]_3$ and $5d[5/2]_3$ excitations are plotted in Fig. 17 and Fig. 18, respectively, for the impact energies 100, 300, and 500 eV together with those transformed from the DCS measurements for 30 eV by Khakoo *et al.* [30]. Present data points for impact energies 100, 300, and 500 eV lie on a

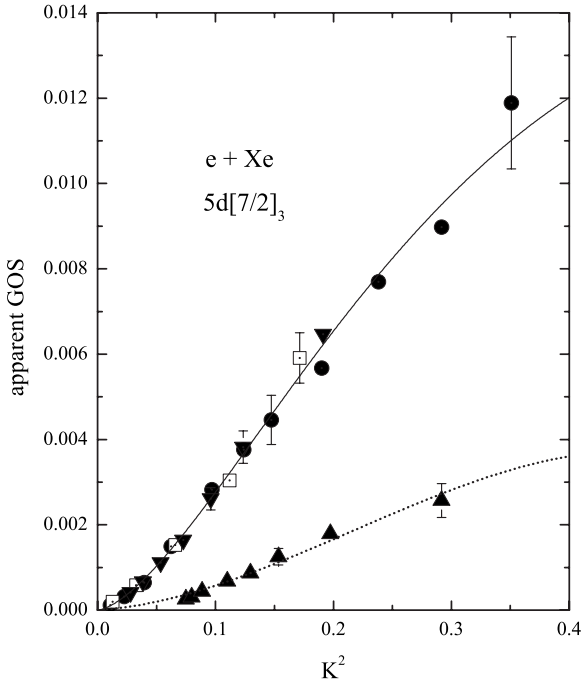

FIG. 17. The apparent GOS for the $5d[7/2]_3$ excitation in Xe as functions of the small K^2 less than 0.4 for 100 (▼), 300 (□), and 500 eV (●) impact energies. Experimental results by Khakoo *et al.* (▲) [30] at 30 eV are also plotted.

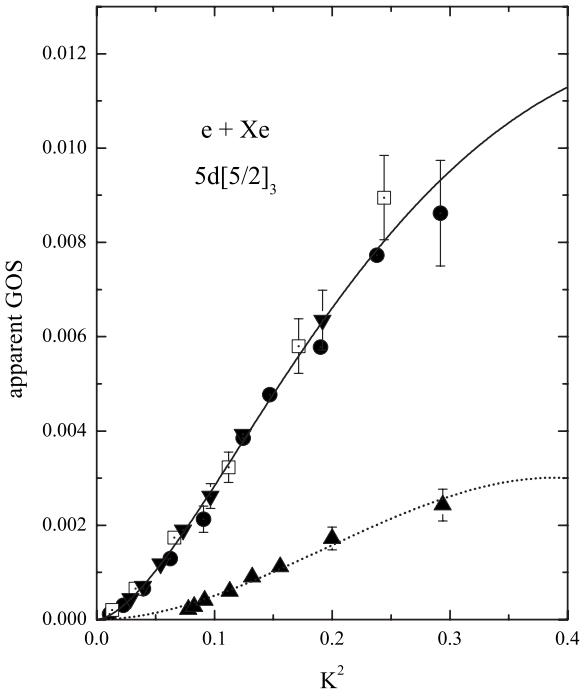

FIG. 18. The apparent GOS for the $5d[5/2]_3$ excitation in Xe as functions of the small K^2 less than 0.4 for 100 (▼), 300 (⊡), and 500 eV (●) impact energies. Experimental results by Khakoo *et al.* (▲) [30] at 30 eV are also plotted.

single curve. The results of Khakoo for 30 eV are much smaller than the present ones, but including them the apparent GOS's have a common shape like a parabola rather than a straight line at small K^2. The experimental errors are presented in Table II.

It has been predicted that the first Born approximation will be held for this transition until impact energy become significantly low, because there exists no intermediate state which connects between the initial and the final states with the dipole matrix element in the second Born amplitude. From our results, it is strongly indicated that the first Born approximation really holds at small K^2 for the impact energies 100–500 eV. As can be seen in Table III, these states are expressed by LS terms $^1F_3$, $^3D_3$, and $^3F_3$, but our experimental results show that no detectable contribution to apparent GOS's from $^3D_3$ and $^3F_3$ components exists and it can be thought that the $^1S_0 \rightarrow {}^1F_3$ transition dominates in these apparent GOS's. From the shapes of the GOS curves, it is judged that the GOS's for the $5d[7/2]_3$ and $5d[5/2]_3$ excitations have the K^4 dependence rather than the K^2 dependence at small K^2 ($\leqslant 0.1$). Therefore, it is supposed that the higher order Born terms mainly contribute to the higher power of K than the fourth. It may be thought that these transitions are dominated by the octupole moment at small scattering angles.

For this transition, the quadrupole moment such as $\langle l|z^2|0\rangle$ vanishes. Therefore, if the first Born approximation is valid, the GOS is proportional to K^4 at small K and is expressed as follows:

$$F_{0l}(K) = 2W|\epsilon_3|^2 K^4, \tag{5}$$

where ϵ_3 stands for an octupole moment, and

$$\frac{1}{3!}\left\langle \psi_f \left| \sum_{s=1}^{N} (\hat{\boldsymbol{K}} \cdot \boldsymbol{r}_s)^3 \right| \psi_0 \right\rangle = \frac{1}{3!}\left\langle \psi_f \left| \sum_{s=1}^{N} (z_s)^3 \right| \psi_0 \right\rangle. \tag{6}$$

$\Sigma_s z_s^3$ can be expressed in terms of zero components of the tensor operators $T_0^{(3)}$ and $T_0^{(1)}$ [31]. Here

$$T_0^{(3)} = -\frac{1}{2} e(5z^3 - 3r^2 z), \tag{7}$$

$$T_0^{(1)} = -ez. \tag{8}$$

Then the GOS is represented as follows [31]:

$$F_{0f}(K) = \{F_{0f}(K)\}_1 + \{F_{0f}(K)\}_2. \tag{9}$$

The first term on the right-hand side of Eq. (9) requires that $\Delta J = 0$ or ± 1 and levels of opposite parity. Therefore, for the present excitations, it vanishes. The second term can be expressed in terms of an electric octupole transition probability A_{eo}

$$\{F_{0f}(K)\}_2 = \frac{3mh^6c^7}{256\pi^6 e^2} \frac{g_f}{g_0} \frac{A_{\mathrm{eo}}}{W^6} K^4 \Delta(J_0 3 J_f), \tag{10}$$

where g_0 and g_f are the statistical weights $2J_0+1$ and $2J_f+1$ of the lower and higher energy levels. Δ denotes a triangular condition which must be satisfied. If the excitation energy W and the momentum transfer K are in atomic units and A_{eo} is in reciprocal seconds, the factor of the coefficient on right-hand side in Eq. (7) is equal to 0.0165.

The present GOS curve in the region of K^2 less than 0.1 for the impact energies 100, 300, and 500 eV have been fitted with a polynomial $\alpha K^4+\beta K^6$. Here α and β are fitting parameters. Using the parameters and Eq. (7), the electric octupole transition probabilities for the $5d[7/2]_3$ and $5d[5/2]_3$ excitations have been estimated roughly. The results are as follows:

$$A_{\mathrm{eo}}(5p^6 \rightarrow 5p^5 5d[7/2]_3) = 8.7(\pm 1.6) \times 10^{-3}(\mathrm{sec}^{-1}),$$

$$A_{\mathrm{eo}}(5p^6 \rightarrow 5p^5 5d[5/2]_3) = 8.9(\pm 1.6) \times 10^{-3}(\mathrm{sec}^{-1}).$$

Unfortunately, experimental or theoretical data for these excitations to be compared with our results are unavailable at present.

Huo [32] obtained the relation between the limiting slope of the apparent GOS curve, $dF_{0l}^{\mathrm{ap}}/dK^2$ and the DCS at $K^2=0$ for dipole forbidden transitions ($\epsilon_1=0$). This is expressed as follows:

$$\lim_{K\rightarrow 0}\left(\frac{dE_{0l}^{\mathrm{ap}}}{dK^2}\right) = \frac{W}{2}\frac{k_f}{k_i}\sigma_{K=0}. \tag{11}$$

For the $5d[7/2]_3$ and $5d[5/2]_3$ excitations, it has been observed that each limiting slope is nearly equal to zero. Consequently, the DCS at $K^2=0$ also should equal to zero. It is suggested that the DCS's observed at small scattering angles decrease as the angle decreases on the way to zero value at $K^2=0$. Such behavior of the DCS's for these transitions can be well understood by using the knowledge of GOS and multipole matrix elements even at considerably low impact energy like 30 eV.

IV. SUMMARY AND CONCLUSIONS

We have measured the apparent GOS's for three types of optically forbidden transitions in rare-gas atoms at small squared momentum transfer K^2 ($\leqslant 0.4$) for the impact energies 100, 300, and 500 eV.

In the excitations of the $2p^5 3p'[1/2]_0$ state in Ne, $3p^5 4p'[1/2]_0$ in Ar, and $4p^5 5p[1/2]_0$ in Kr from the ground $np^6 {}^1S_0$ state, the curves of the apparent GOS's reveal the distinct behavior of the impact energy dependence, characteristic of the ${}^1S \rightarrow {}^1S$ type excitation, e.g., $1\,{}^1S_0 \rightarrow 2\,{}^1S_0$ excitation in He. The apparent GOS curve asymptotically approaches the curve calculated by the first Born approximation (Bethe-GOS curve) as the impact energy increases. Inversely, when the impact energy decreases, the apparent GOS curve departs from the Born curve, increasing at K^2 smaller than 0.15 to 0.2 a.u. and having a small maximum at the K^2 region from 0.1 to 0.03 a.u. Though the states mentioned above cannot be expressed only by the pure ${}^1S_0$ term but contain some components of other terms like ${}^3P_0$, our experimental results suggest that this feature may be characteristic of the ${}^1S_0 \rightarrow {}^1S_0$ transitions in atoms.

As for the $np^5(n+1)p[5/2]_{2,3}$ and $np^5(n+1)p[3/2]_{1,2}$ transitions in Ar, Kr, and Xe, in which the final states are represented as the linear combination of the ${}^3D_2$, ${}^1D_2$, and ${}^3P_2$ terms, an overall tendency in the impact energy dependence of the apparent GOS curves has been observed as follows: The apparent GOS's have larger values for lower impact energies and decrease as the impact energy increases approaching the Bethe-GOS's, in contrast to the case of the ${}^1S \rightarrow {}^1S$ type transition. In other words, the apparent GOS curve situates at higher position for the low impact energy and moves to lower position as the impact energy increases. It is found that this tendency of the impact energy dependence is clearly reproduced in the apparent GOS curves for the $1\,{}^1S_0 \rightarrow 3\,{}^1D_2$ excitation in He, which were deduced from DCS's obtained by theoretical calculations by several authors. This suggests that the transitions here resulted dominantly from the ${}^1S_0 \rightarrow {}^1D_2$ type transition that is the electric quadrupole transition.

However, rather remarkable variations have been observed in the shape of the apparent GOS curves and in the manner how the curves approach the Bethe-GOS curve, depending on the respective final states and the atomic species. These discrepancies from the simple ${}^1S_0 \rightarrow {}^1D_2$ type transition might be partly attributable to transitions to the ${}^3P_2$ or ${}^3D_2$ components and to unresolved $[5/2]_3$ or $[3/2]_1$ state, although no clear interpretations are available for the present.

The characteristic behavior of the DCS and the apparent GOS for the $5p^5 5d[7/2]_3$ and $5p^5 5d[5/2]_3$ transitions in Xe, in which the final states expressed by the linear combination of the ${}^1F_3$, ${}^3D_3$, and ${}^3F_3$ terms, have been observed in detail at small K^2 ($\leqslant 0.1$). The apparent GOS curves for the both transitions have been no impact energy dependence for the impact energies 100–500 eV at small K^2 ($\leqslant 0.4$). The profile of the apparent GOS curves shows a parabola rather than a straight line at small K^2 region. It is suggested that the present GOS curves show the characteristic behavior of the ${}^1S_0 \rightarrow {}^1F_3$ type transition, in which the transition by the octupole moment is dominant. The electric octupole transition probabilities for the $5d[7/2]_3$ and the $5d[5/2]_3$ excitations have been estimated from the experimental results of the GOS functions in the $K^2 \rightarrow 0$ region.

ACKNOWLEDGMENT

We would like to acknowledge Dr. Mitio Inokuti, a senior physicist of Argonne National Laboratory, for valuable discussions.

[1] H. Bethe, Ann. Phys. **5**, 325 (1930).
[2] A comprehensive review by Inokuti is a classic. M. Inokuti, Rev. Mod. Phys. **43**, 297 (1971).
[3] T. Y. Suzuki, H. Suzuki, S. Ohtani, B. S. Min, T. Takayanagi, and K. Wakiya, Phys. Rev. A **49**, 4578 (1994).
[4] G. P. Li, T. Takayanagi, K. Wakiya, H. Suzuki, T. Ajiro, S. Yagi, S. S. Kano, and H. Takuma, Phys. Rev. A **38**, 1240 (1988).
[5] T. Takayanagi, G. P. Li, K. Wakiya, H. Suzuki, T. Ajiro, T. Inaba, S. S. Kano, and H. Takuma, Phys. Rev. A **41**, 5948 (1990).
[6] T. Y. Suzuki, Y. Sakai, B. S. Min, T. Takayanagi, K. Wakiya, H. Suzuki, T. Inaba, and H. Takuma, Phys. Rev. A **43**, 5867 (1991).
[7] T. Y. Suzuki, H. Suzuki, F. J. Currell, S. Ohtani, T. Takayanagi, and K. Wakiya, Phys. Rev. A **53**, 4138 (1996).
[8] C. E. Moore, *Atomic Energy Levels*, Natl. Bur. Stand. (U.S.) Circ. No. 467 (U.S. GPO, Washington, D.C., 1958), Vols. I, II, III.
[9] T. Y. Suzuki, H. Suzuki, F. J. Currell, S. Ohtani, Y. Sakai, T. Takayanagi, and K. Wakiya, Phys. Rev. A **57**, 1832 (1998).
[10] W. A. Goddard III, D. L. Huestis, D. C. Cartwright, and S. Trajmar, Chem. Phys. Lett. **11**, 329 (1971).
[11] M. A. Khakoo, S. Trajmar, L. R. LeClair, I. Kanik, G. Csanak, and C. J. Fontes, J. Phys. B **29**, 3455 (1996).
[12] Y. Fujita, S. Yagi, S. S. Kano, H. Takuma, T. Ajiro, T. Takayanagi, K. Wakiya, and H. Suzuki, Phys. Rev. A **34**, 1568 (1986).
[13] K. Jost, J. Phys. E **12**, 1006 (1979).
[14] R. W. Wagenaar, A. de Boer, T. van Tubergen, J. Los, and F. J. de Heer, J. Phys. B **19**, 3121 (1986).
[15] R. H. Jansen, F. J. de Heer, H. J. Luyken, B. van Wingerden, and H. J. Blaaun, J. Phys. B **9**, 185 (1976).
[16] R. H. Jansen and F. J. de Heer, J. Phys. B **9**, 213 (1976).
[17] J. P. Bromberg, J. Chem. Phys. **61**, 963 (1974).
[18] V. F. Register and S. Trajmar, Phys. Rev. A **29**, 1785 (1984).
[19] S. C. Gupta and J. A. Rees, J. Phys. B **8**, 417 (1975).
[20] M. A. Dillon and E. N. Lassettre, J. Chem. Phys. **62**, 2373 (1975).
[21] S. F. Register, S. Trajmar, G. Steffensen, and D. C. Cartwright, Phys. Rev. A **29**, 1793 (1984).
[22] Hua-Dong Cheng, Lin-Fan Zhu, Zhen-Sheng Yuan, Xiao-Jing Liu, Jian-Min Sun, Wei-Chun Jiang, and Ke-Zun Xu, Phys. Rev. A **72**, 012715 (2005).
[23] A. Chutjian and D. C. Cartwright, Phys. Rev. A **23**, 2178 (1981).
[24] Lin-Fan Zhu, Hua-Dong Cheng, Zhen-Sheng Yuan, Xiao-Jing Liu, Jian-Min Sun, and Ke-Zun Xu, Phys. Rev. A **73**, 042703 (2006).
[25] Wen-bin Li, Lin-fan Zhu, Xiao-jing Liu, Zhen-sheng Yuan, Jian-min Sun, Hua-dong Cheng, Zhi-ping Zhong, and Ke-zun Xu, Phys. Rev. A **67**, 062708 (2003).
[26] A. Skerbele and E. N. Lassettre, J. Chem. Phys. **53**, 3806 (1970).
[27] E. N. Lassettre and A. Skerbele, J. Chem. Phys. **54**, 1597 (1971).
[28] K. H. Winters, M. Issa, and B. H. Bransden, Can. J. Phys. **55**, 1074 (1977).
[29] Hua-Dong Cheng, Lin-Fan Zhu, Xiao-Jing Liu, Zhen-Sheng Yuan, Wen-Bin Li, and Ke-Zun Xu, Phys. Rev. A **71**, 032714 (2005).
[30] M. A. Khakoo, S. Trajmar, S. Wang, I. Kanik, A. Aguirre, C. J. Fontes, R. E. H. Clark, and J. Abdallah, Jr., J. Phys. B **29**, 3477 (1996).
[31] R. H. Garstang, J. Phys. B **1**, 847 (1968).
[32] W. M. Huo, J. Chem. Phys. **71**, 1593 (1979).
[33] L. E. Machado, E. P. Leal, and G. Csanak, Phys. Rev. A **29**, 1811 (1984).
[34] Xuezhe Guo, D. F. Mathews, G. Mikaelian, M. A. Khakoo, A. Crowe, I. Kanik, S. Trajmar, V. Zeman, K. Bartschat, and C. J. Fontes, J. Phys. B **33**, 1921 (2000).